15th Canadian Masonry Symposium
Ottawa, Canada
June 2-5, 2025

3D Microstructure Generation of Rubble Stone Masonry Walls from 2D Images

Qianqing Wang[i], **Katrin Beyer**[ii]

ABSTRACT

Microscale modeling of rubble stone masonry structures is hindered by the lack of geometric data on the microstructure, including units' shapes and arrangement in 3D. This paper introduces an automated method for generating synthetic 3D models of rubble stone masonry walls using photos of real walls. The process involves identifying geometric parameters from 2D stone shapes in the segmented wall photos, and generating 3D stones with these parameters based on spherical harmonics. A geometric planning algorithm, mimicking the construction process of masons, is then used to assemble the generated stones, creating multi-leaf masonry walls. We use the method for a case study, where a wall of size 1600 mm × 1600 mm × 400 mm is created from the photo of the façade of a real wall. The generated wall is compared to the real wall using indices that quantify the geometric features of units, including size, aspect ratio and sphericity. The arrangement of stones is also compared in terms of vertical interlocking and course horizontality, demonstrating similarity between the synthetic and real structures.

KEYWORDS

Rubble stone masonry, microstructure, spherical harmonics, typology generator

[i] PhD candidate, EESD, EPFL, Lausanne, Switzerland, qianqing.wang@epfl.ch
[ii] Associate Professor, EESD, EPFL, Lausanne, Switzerland, katrin.beyer@epfl.ch

INTRODUCTION

Stone masonry is one of the oldest construction materials and has been widely used in heritage structures [1]. However, these structures are often vulnerable to damage during earthquakes, highlighting the importance of understanding their seismic behavior [2, 3]. Unlike brick masonry, stone masonry typically features irregular shapes and patterns which complicate structural analysis [1,4]. Numerical modeling approaches that explicitly capture geometric details at the stone level (i.e. microscale modeling) can incorporate these irregularities to accurately simulate real-world conditions [4].

However, detailed or simplified micro-models require proper geometric definition of masonry patterns due to their influence on structural response [1]. One of the challenges in conducting simulations at microscale is the lack of geometric data about the microstructure, i.e. the shape and size of each stone and its position within the wall [5]. Therefore, many of the works are limited to 2D modeling. Synthetic 2D walls are used in [1], in which bricks are generated from surveying real walls and arranged by an algorithm with an interlocking parameter. For irregular units, Zhang and Beyer [2] generate walls with irregular units according to the typology classification in the Italian code. To generate textures for a specific wall, one needs to calibrate the input parameters by trial-and--error. Apart from generating synthetic walls, one can obtain the geometry of units directly by segmenting the façade of the wall and creating simplified [4] or detailed [3] microscale models.

For 3D modeling, one needs to either build the digital twin simultaneously with the physical construction or generate synthetic walls. Saloustros et al. [5] build the geometric digital twin of three stone masonry walls by scanning the stones and recording their positions in the wall during construction. The final output explicitly replicates the geometry of the wall down to the detail of individual stones. For generating synthetic walls, Pereira et al. [6] create three-leaf walls composed of cuboid-shaped blocks, the dimensions of which are sampled from windows on real walls. Shaqfa and Beyer [7] developed a 3D virtual typology generator for masonry walls. The units are generated from a sequence of operations including mesh refinement, noise addition, and Laplacian smoothing. The stones are assembled in a manner similar to physical construction by masons. However, the units and the walls are compared to real walls visually without an objective, quantitative comparison.

In this work, we develop an automated process to generate synthetic 3D walls from photos of real walls. We parameterize unit shapes segmented from a wall photo using spherical harmonics and generate 3D stones with the parameters. The generated stones are assembled through a stacking algorithm, which mimics masons' behaviour and generates multi-leaf masonry walls. We generate a three-leaf masonry wall as a case study and compare the results with real walls.

STONE GENERATION

Fig. 1 illustrates the proposed stone generation process. It starts from generating ranges of geometric characteristics for stone shapes from the segmented photo of the wall. The ranges are used to randomly sample shape parameters that feed a shape generator based on spherical harmonics (SH) to generate 3D shapes. In the following, we present first the spherical harmonics shape generator and its necessary input. Then the method to estimate parameter ranges from wall photos is described.

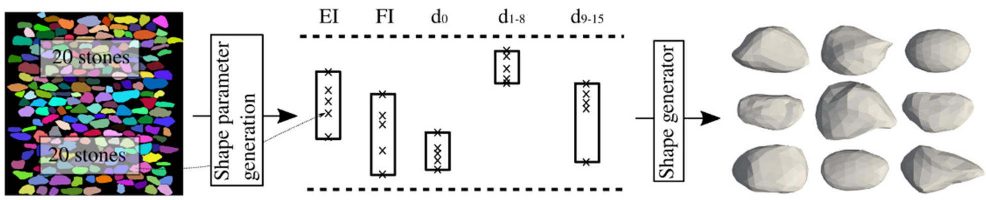

Figure 1: The generation of 3D stones using a segmented wall photo.

Shape generation using spherical harmonics

The coordinates of the vertices on a particle surface can be represented by spherical harmonic expansion as:

$$(1)\quad \begin{pmatrix} x(\theta,\phi) \\ y(\theta,\phi) \\ z(\theta,\phi) \end{pmatrix} = \begin{pmatrix} \sum_{l=1}^{l_{\max}} \sum_{m=-l}^{l} c_{x,l}^{m} Y_l^m(\theta,\phi) \\ \sum_{l=1}^{l_{\max}} \sum_{m=-l}^{l} c_{y,l}^{m} Y_l^m(\theta,\phi) \\ \sum_{l=1}^{l_{\max}} \sum_{m=-l}^{l} c_{z,l}^{m} Y_l^m(\theta,\phi) \end{pmatrix}$$

where Y_l^m and (c_x^m, c_y^m , c_z^m) are the spherical harmonic (SH) and coefficients of degree l and order m, respectively. $l_{\max}$ is the maximum SH degree used to reconstruct a particle surface. The shape features at an SH degree of l are characterized by

$$(2)\quad \begin{pmatrix} x_j(\theta,\phi) \\ y_j(\theta,\phi) \\ z_j(\theta,\phi) \end{pmatrix} = \begin{pmatrix} \mathrm{c}_{\mathrm{x,j}}^{-\mathrm{l}} & \mathrm{c}_{\mathrm{x,j}}^{-\mathrm{l}+1} & \cdots & \mathrm{c}_{\mathrm{x,j}}^{\mathrm{l}} \\ \mathrm{c}_{\mathrm{y,j}}^{-\mathrm{l}} & \mathrm{c}_{\mathrm{y,j}}^{-\mathrm{l}+1} & \cdots & \mathrm{c}_{\mathrm{y,j}}^{\mathrm{l}} \\ \mathrm{c}_{\mathrm{z,j}}^{-\mathrm{l}} & \mathrm{c}_{\mathrm{z,j}}^{-\mathrm{l}+1} & \cdots & \mathrm{c}_{\mathrm{z,j}}^{\mathrm{l}} \end{pmatrix} \begin{pmatrix} \mathrm{Y}^{-\mathrm{l}}(\theta,\phi) \\ \mathrm{Y}^{-\mathrm{l}+1}(\theta,\phi) \\ \vdots \\ \mathrm{Y}^{\mathrm{l}}(\theta,\phi) \end{pmatrix} = C_j Y_l(\theta,\phi)$$

where C_j is a $3 \times (2l-1)$ dimensional matrix including the SH coefficients of degree l.

Zhao et al. [8] showed that the SH coefficients can be reconstructed using the following equations:

$$(3)\quad C_1 = \sqrt{\frac{\pi}{6}} \begin{pmatrix} -\mathrm{E}I \times i & 0 & \mathrm{E}I \times i \\ 0 & \sqrt{2\mathrm{E}I \times \mathrm{F}I} & 0 \\ 0 & 0 & 0 \end{pmatrix}$$

$$(4)\quad C_l = \begin{pmatrix} c_{x,j}^{-l} & \cdots & c_{x,j}^{0} & \cdots & c_{x,j}^{l} \\ c_{y,j}^{-l} & \cdots & c_{y,j}^{0} & \cdots & c_{y,j}^{l} \\ c_{z,j}^{-l} & \cdots & c_{z,j}^{0} & \cdots & c_{z,j}^{l} \end{pmatrix} = \begin{pmatrix} k_x(\alpha_{2l} - \alpha_{2l+1} i) & \cdots & k_x \alpha_1 & \cdots & k_x(\alpha_{2l} + \alpha_{2l+1} i) \\ k_y(\beta_{2l} - \beta_{2l+1} i) & \cdots & k_y \beta_1 & \cdots & k_y(\beta_{2l} + \beta_{2l+1} i) \\ k_z(\epsilon_{2l} - \epsilon_{2l+1} i) & \cdots & k_z \epsilon_1 & \cdots & k_z(\epsilon_{2l} + \epsilon_{2l+1} i) \end{pmatrix}$$

$$(5)\quad k_x = \sqrt{\frac{d_{x,l}^2}{\alpha_1^2 + 2\sum_{i=2}^{2l+1} \alpha_i^2}},\ k_y = \sqrt{\frac{d_{y,l}^2}{\alpha_1^2 + 2\sum_{i=2}^{2l+1} \alpha_i^2}},\ k_z = \sqrt{\frac{d_{z,l}^2}{\alpha_1^2 + 2\sum_{i=2}^{2l+1} \alpha_i^2}}$$

$$(6)\quad d_{x,l} = d_{y,l} = d_{z,l}$$

where i is the imaginary unit, $(\alpha_i, \beta_i, \epsilon_i)$ for $i \in [1, 2l+1]$ are real numbers between 0 and 1, which are randomly generated with a uniform distribution. k_x, k_y and k_z are three normalizing factors. $d_{x,l}$, $d_{y,l}$ and $d_{z,l}$ are the three components of the spherical descriptors d_l , which following the following correlations across different degrees

(7) $d_l = \begin{cases} d_2 \cdot \left(\frac{2}{l}\right)^{\alpha}, \text{for } l \in [2,8] \\ d_9 \cdot \left(\frac{9}{l}\right)^{\beta}, \text{for } l \in [9,15] \end{cases}$

α and β are fitted values, ranging between [1.320, 1.448] and [1.190, 1.672] for 40 random particles studied by Zhao et al. [8]. We used the same fitted value to generate our stones (1.387 and 1.426) as for Leighton Buzzard sand particles [9]. The coefficient matrices for SH degrees between 2 and 15 can be constructed from two specified value of d_{2-8}/d_1 and d_{9-15}/d_1, defined as:

(8) $d_{2-8}/d_1 = \sum_{l=2}^{8} \frac{d_l}{d_1}$

(9) $d_{9-15}/d_1 = \sum_{l=9}^{15} \frac{d_l}{d_1}$

With Eq. (1) - Eq. (9), a particle shape can be reconstructed using four factors, namely the elongation index EI, the flatness index FI, d_{2-8}/d_1 and d_{9-15}/d_1. The size of the particle is controlled by d_1.

Shape parameter generation

In this section, we present the method to estimate the ranges of input parameters for the spherical harmonics-based particle generator, including EI, FI, and d_1 from a segmented image of the facade of the wall. The elongation index EI and the flatness index FI of a 3d shape can be estimated from its 2d projections with the method proposed by Wang et al. [10]. To estimate EI and FI for a 3D stone given its projected photos, one first measures the semi-length of the major and minor axes of the enveloped rectangle (r_1 and r_2) for each projection using the bounding box method. With n projections, the elongation and flatness are estimated using Eq. (10):

(10)
$$\mathrm{EI} = \frac{r_{\mathrm{mean}}}{r_{1\mathrm{max}}},\ \mathrm{FI} = \frac{r_{2\mathrm{min}}}{r_{\mathrm{mean}}}$$
$$r_{\mathrm{mean}} = (r_{1\mathrm{min}} + r_{2\mathrm{max}})/2$$
$$r_{1\mathrm{max}} = \max(r_{11}, r_{1i}, \dots, r_{1n})$$
$$r_{1\mathrm{min}} = \min(r_{11}, r_{1i}, \dots, r_{1n})$$
$$r_{2\mathrm{max}} = \max(r_{21}, r_{2i}, \dots, r_{2n})$$
$$r_{2\mathrm{min}} = \min(r_{21}, r_{2i}, \dots, r_{2n})$$

It is shown that with 5-20 projections, one can obtain a good estimation of EI and FI of the 3D shape [10]. We adapt this method to estimate the range of EI, FI for a group of stones observed in a single projection. We assume that the projection of different stones from the same angle is equivalent to the projection of a single stone from different angles. Therefore, instead of taking n projections of a single stone, we use n segmented stones from the facade of the wall to estimate the flatness and elongation of one stone using Eq. (10). We estimate the flatness and elongation 100 times, each time with 20 randomly selected stones. Based on the 100 estimations, we obtain the maximal and minimal bound for EI and FI.

The stone size parameter d_1, which can be interpreted as the maximal dimension of the stone, is estimated using $r_{1\mathrm{max}}$. Its range is estimated in the same way as EI and FI.

For d_{2-8}/d_1 and d_{9-15}/d_1 that are related to the angularity and convexity of the generated shape, we select ranges to [0, 0.3] and [0, 0.1] by trial and error, respectively, based on a trial-and-error approach.

Stones generated with values exceeding these upper limits tend to exhibit acute angles and artifacts. With these ranges, we uniformly sample input parameters and generate stones using the SH generator.

STONE STACKING

We use the geometric planning method for constructing multi-leaf masonry walls with irregular stones proposed in [11]. The generation of a wall is formulated as a sequential process, which begins with a stone stock composed of generated stones, flat ground and predefined borders. At each step, a stone stacking algorithm determines the optimal placement for a stone. This involves a hierarchical filtering process that uses discrete convolution operations between 3D tensors representing the landscape (including the ground, borders, and already placed stones) and the stones to rule out infeasible positions. The filtering process checks for overlaps, contact with other stones, and compliance with traditional masonry rules. These rules include ensuring stones are placed within the maximum height of previous stones, avoiding vertical placement near borders, and staggering vertical head joints for good interlocking. After filtering, a multi-objective optimization process is used to find the best position for the stone. This optimization takes into account the proximity to the landscape, stone height, and distance to the bottom corner of the landscape. The algorithm allows for trial placement of multiple stones and selects the best one out of them. The best stone is chosen based on a weighted sum of geometric factors, including height, proximity, contact with multiple stones, interlocking, and compliance with masonry rules. Finally, the selected stone is placed, updating the landscape for the next iteration.

RESULTS

We benchmark the wall generation method against the physical walls built in [12], where 1600 mm × 1600 mm × 400 mm rubble stone masonry walls are built by skilled masons. Fig. 2 shows the photo of the walls and the segmented image of one of the façades of the wall. The segmentation of the stones is realized by using the open-source tool Segment Anything Model (SAM) [13] for a rough segmentation followed by manual correction.

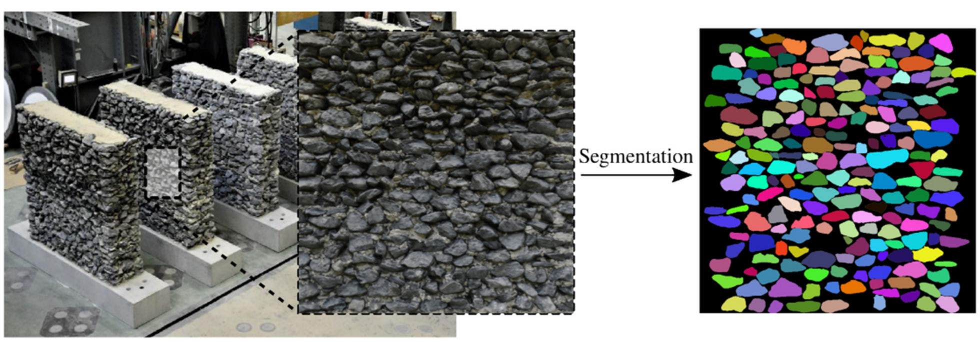

Figure 2: Segmentation of stones from wall photo. Figures adapted from [12]. The wall facade photo is generated from the wall surface model with textures in [14].

Fig. 3(a) illustrates the distribution of generated stone shapes in the elongation-flatness space, with volume of stone annotated by color. Fig. 3(b) depicts examples of generated stones. Stones are concentrated in an elongation range (0.66,1) and in a flatness range (0.2,0.75).

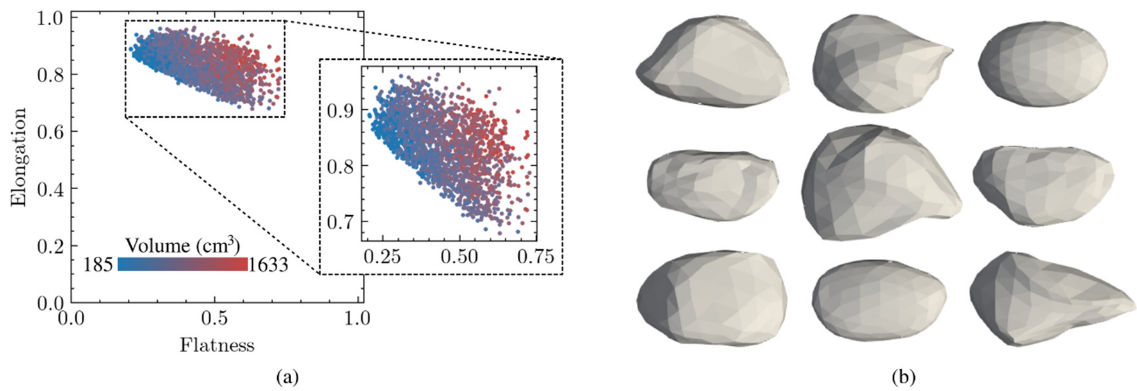

Figure 3: Generated stones. (a) Distribution of stone shapes in elongation-flatness space. Volume of stones is annotated by color. (b) Examples of generated stones.

In the wall generation process, stone meshes are voxelized with voxels of 1 cm in edge length. Stones are initially orientated such that the main axis are aligned with the global x-y-z axis. 24 orientations with 90-degree interval are considered for each stone. In each step, 1 randomly selected stone is stacked. We use the same dimension as the real wall to set the borders for stone stacking. Figure 4 shows the generated wall. The wall is composed of 716 stones. The color of the stones indicates the stacking sequence, with blue representing the stones placed first and red representing those placed later.

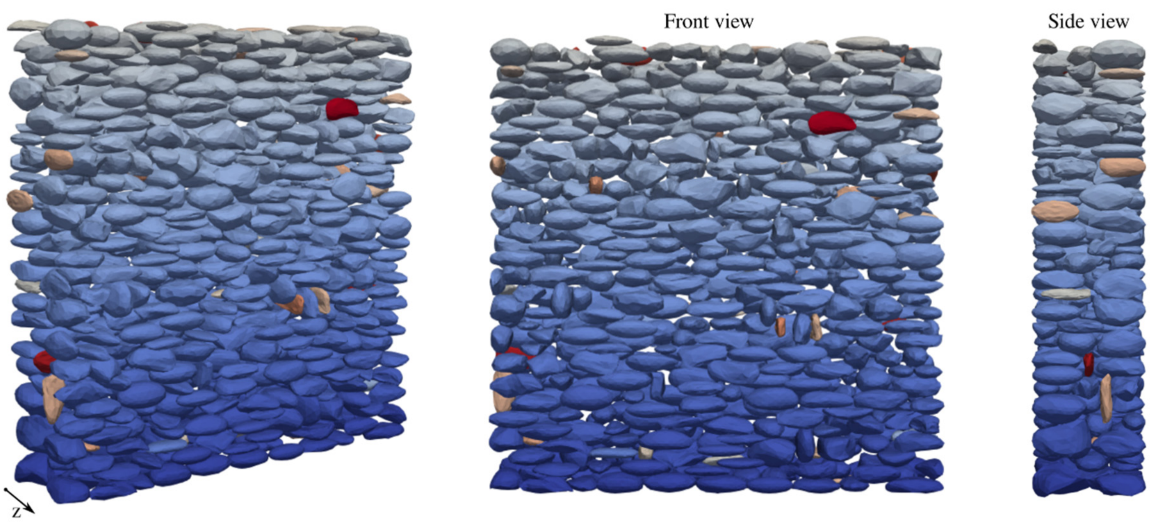

Figure 4: A 1.6 m × 1.6 m × 0.4 m wall generated with synthetic stones.

To quantitatively verify the similarity between the generated wall and the real wall, we compare unit shapes and unit arrangement of the two walls. As the real wall can only be evaluated through the photo of the façade, we quantify the geometric characteristics through indices that can be evaluated on 2D images. For the generated wall, we create slices of the wall at z=70 mm, which locates at the maximum of stone-to-wall ratio across the thickness. We use three indices to quantify unit shapes, namely:

- Radius: It is the radius of the circle that has the same area as the shape.

- Aspect ratio: It is usually used for 2-dimensional description of the form of particles, computed as the ratio of the major axis to minor axis of the ellipse equivalent to the object.
- Sphericity: It is inspired by the definition of sphericity in [9] for 3D shapes, evaluating the deviation of a 3D shape to a sphere. Here we propose a 2D sphericity as the ratio between the perimeter of the area-equivalent circle and the perimeter of the shape, to evaluate the deviation of a 2d shape to a circular shape:

(11) $$\mathrm{SP} = \frac{\sqrt{8\pi A}}{p}$$

where p and A are the perimeter and area of the particle shape.

Figure 5 shows the distribution of the three indices for stones on the photo of real wall compared to the distribution of indices for stones on the slice of the generated wall. The stones on the two walls are similar in terms of the range and distribution of size, aspect ratio and sphericity.

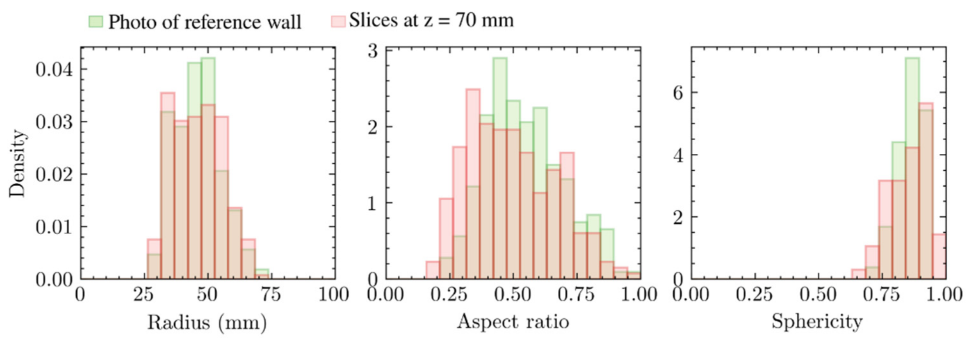

Figure 5: Distribution of stone properties on the exterior surface of the generated wall compared to stones in the wall photo.

Four indices are used to compare the arrangement of units, including:

- Vertical alignment (F_{AV}): The vertical alignment factor assesses the vertical joint interlocking between courses [15]. It is calculated using the following equation:

(12) $$F_{AV} = \frac{1}{n}\sum_{i=1}^{n}\frac{v_i - h_{wall}}{h_{wall}}$$

where v_i is the length of the shortest path along the vertical joints between two points located at the top and the bottom edge of the wall with the same horizontal coordinate. h_{wall} is the height of the wall. We take five pairs of points for evaluation and use the average value for comparison.
- Horizontal alignment (F_{AH}): The horizontality of the bed joints is usually evaluated using the horizontal alignment factor [15], defined as:

(13) $$F_{AH} = \frac{1}{n}\sum_{i=1}^{n}\frac{h_i - w_{wall}}{w_{wall}}$$

where h_i is the shortest path length along the horizontal joints between two points located at the same vertical position on the left and right boundaries of the wall, respectively. w_{wall} is the length of the wall in the y direction. Similar to F_{AV}, we evaluate five paths and use the average value for comparison.
- Diagonal line of minimum trace: It evaluates the length of the shortest paths along the diagonals of the wall, written as follows [16]:

(14) $$\mathrm{LMT(diag\text{-}pos)} = \frac{\text{shortest length between left top corner and right bottom corner through mortar}}{\text{direct distance between the two corners}}$$

$$\text{(15)} \qquad \mathrm{LMT(diag\text{-}neg)} = \frac{\text{shortest length between right top corner and left bottom corner through mortar}}{\text{direct distance between the two corners}}$$

LMT(diag-pos) and LMT(diag-neg) are two indices strongly correlated with the strength of the wall (loaded in positive direction and in negative direction, respectively) when it fails in shear failure [11].

Table 1 compares the three indices for the generated wall at slice z=70mm and the real wall, demonstrating that the stone arrangement of the two walls is quite similar.

Table 1: Comparison of unit arrangement between the generated wall and the real wall.

Wall	$\mathbf{F_{AV}}$ **(%)**	$\mathbf{F_{AH}}$ **(%)**	LMT(diag-pos)	LMT(diag-neg)
Generated wall (slice at z=70mm)	20.0	2.7	1.10	1.10
Real wall (photo of the facade)	19.6	4.3	1.09	1.11

CONCLUSIONS

This paper presents a novel, automated method for generating the microstructure of rubble stone masonry walls from photos of real walls, addressing a critical gap in geometric data for microscale analysis. By combining spherical harmonics-based shape generation with a masonry-inspired stacking algorithm, our approach produces synthetic walls that quantitatively match real structures in unit geometry and arrangement. The method enables practical advances in seismic assessment, providing the geometric foundation for microscale simulations to predict failure mechanisms in historic masonry. Future work will integrate material properties for nonlinear analysis and extend the framework to other masonry typologies, further bridging the gap between image-based surveys and 3D modeling for engineering and conservation applications.

REFERENCES

[1] Simon Szabó, Marco Francesco Funari, and Paulo B. Lourenço. "A mason-inspired pattern generator for historic masonry structures using quality indexes". In: Engineering Structures 304 (Apr. 2024), p. 117604. issn: 0141-0296. doi: 10.1016/j.engstruct.2024.117604. url: http://dx.doi.org/10. 1016/j.engstruct.2024.117604.

[2] Shenghan Zhang, Martin Hofmann, and Katrin Beyer. "A 2D typology generator for historical masonry elements". In: Construction and Building Materials 184 (Sept. 2018), 440–453. issn: 0950-0618. doi: 10.1016/j.conbuildmat.2018.06.085. url: http://dx.doi.org/10.1016/j.conbuildmat.2018. 06.085.

[3] Tomas Krejci et al. "Effective elastic and fracture properties of regular and irregular masonry from nonlinear homogenization". In: Computers amp; Structures 254 (Oct. 2021), p. 106580. issn: 0045-7949. doi: 10.1016/j.compstruc.2021.106580. url: http://dx.doi.org/10.1016/j.compstruc.2021. 106580.

[4] Yahroun Fei Long Hermans et al. "Efficient image-based homogenized limit analysis for irregular masonry with lumped mortar joints representation". In: Engineering Structures 318 (Nov. 2024), p. 118688. issn: 0141-0296. doi: 10.1016/j.engstruct.2024.118688. url: http://dx.doi.org/10.1016/j. engstruct.2024.118688.

[5] Savvas Saloustros et al. "Geometrical digital twins of the as-built microstructure of three-leaf stone masonry walls with laser scanning". In: Scientific Data 10.1 (Aug. 2023). issn: 2052-4463. doi: 10. 1038/s41597-023-02417-3. url: http://dx.doi.org/10.1038/s41597-023-02417-3.

[6] M. Pereira et al. "Automatic multi-leaf nonperiodic block-by-block pattern generation and computational analysis of historical masonry structures". In: Engineering Structures 283 (May 2023),

p. 115945. issn: 0141-0296. doi: 10.1016/j.engstruct.2023.115945. url: http://dx.doi.org/10.1016/j.engstruct.2023.115945

[7] Mahmoud Shaqfa and Katrin Beyer. “A virtual microstructure generator for 3D stone masonry walls”. In: European Journal of Mechanics - A/Solids 96 (Nov. 2022), p. 104656. issn: 0997-7538. doi: 10.1016/j.euromechsol.2022.104656. url: http://dx.doi.org/10.1016/j.euromechsol.2022.104656.

[8] B. D. Zhao, D. H. Wei, and J. F. Wang. “Particle shape quantification using rotation-invariant spherical harmonic analysis”. In: G´eotechnique Letters 7.2 (June 2017), 190–196. issn: 2045-2543. doi: 10.1680/ jgele.17.00011. url: http://dx.doi.org/10.1680/jgele.17.00011.

[9] Deheng Wei, Jianfeng Wang, and Budi Zhao. “A simple method for particle shape generation with spherical harmonics”. In: Powder Technology 330 (May 2018), 284–291. issn: 0032-5910. doi: 10.1016/ j.powtec.2018.02.006. url: http://dx.doi.org/10.1016/j.powtec.2018.02.006.

[10] Xiang Wang et al. “Superellipsoid-based study on reproducing 3D particle geometry from 2D projections”. In: Computers and Geotechnics 114 (Oct. 2019), p. 103131. issn: 0266-352X. doi: 10.1016/j. compgeo.2019.103131. url: http://dx.doi.org/10.1016/j.compgeo.2019.103131.

[11] Qianqing Wang, Ketson R.M. dos Santos, and Katrin Beyer. “Geometric Planning for Masonry Wall Construction with Natural Stones Using Discrete Convolution”. In: Engineering Structures 329 (April 2025), 119695. url: http://dx.doi.org/10.1016/j.engstruct.2025.119695.

[12] Amir Rezaie, Michele Godio, and Katrin Beyer. “Experimental investigation of strength, stiffness and drift capacity of rubble stone masonry walls”. In: Construction and Building Materials 251 (Aug. 2020), p. 118972. issn: 0950-0618. doi: 10.1016/j.conbuildmat.2020.118972. url: http://dx.doi.org/10.1016/j.conbuildmat.2020.118972.

[13] Alexander Kirillov et al. Segment Anything. 2023. arXiv: 2304.02643 [cs.CV]. url: https://arxiv.org/abs/2304.02643.

[14] Amir Rezaie, Michele Godio and Katrin Beyer, “Experimental data on plastered rubble stone masonry walls”. Zenodo, (Jul. 01, 2021). doi: 10.5281/zenodo.5052675.

[15] Celeste Almeida et al. “Geometric indices to quantify textures irregularity of stone masonry walls”. In: Construction and Building Materials 111 (May 2016), 199–208. issn: 0950-0618. doi: 10.1016/j.conbuildmat.2016.02.038. url: http://dx.doi.org/10.1016/j.conbuildmat.2016.02.038.

[16] Shenghan Zhang and Katrin Beyer. “Numerical investigation of the role of masonry typology on shear strength”. In: Engineering Structures 192 (Aug. 2019), 86–102. issn: 0141-0296. doi: 10 . 1016 / j . 125 engstruct.2019.04.026. url: http://dx.doi.org/10.1016/j.engstruct.2019.04.026.